Interaction between coronal mass ejections and the solar wind

Jones, R. A.; Breen, A. R.; Fallows, R. A.; Canals, A.; Bisi, M. M.; Lawrence, G.

Published in:
Journal of Geophysical Research: Space Physics

DOI:
10.1029/2006JA011875

Publication date:
2007

Citation for published version (APA):
Jones, R. A., Breen, A. R., Fallows, R. A., Canals, A., Bisi, M. M., & Lawrence, G. (2007). Interaction between coronal mass ejections and the solar wind. *Journal of Geophysical Research: Space Physics*, *112*(A8), 8107. https://doi.org/10.1029/2006JA011875

Interaction between coronal mass ejections and the solar wind

R.A. Jones, A.R. Breen, R.A. Fallows, A. Canals[1]

Institute of Mathematical and Physical Sciences, University of Wales, Aberystwyth

M.M. Bisi[1]

Center for Astrophysics and Space Sciences, University of California, San Diego

G. Lawrence

Department of Solar Physics, Royal Observatory of Belgium

Short title: IPS OBSERVATIONS OF ICMES

[1]At University of Wales, Aberystwyth when the work described in this paper was carried out

Abstract. Observations suggest that the interplanetary extensions of Coronal Mass Ejections (iCMEs) may be accelerated or decelerated in their passage through the solar wind. Interplanetary scintillation measurements (IPS) can detect the passage of iCMEs beyond the field of view of the Large-Angle and Spectrometric Coronagraph (LASCO) coronagraphs and can provide information on their velocities. The European Incoherent SCATter Radar (EISCAT) and the Multi Element Radio Linked Interferometer Network (MERLIN) systems, with a field of view covering 10 to 120 solar radii, can provide information on iCMEs in the inner regions of the solar wind. IPS observations can also provide solar wind velocity measurements ahead of the iCME, and using this information we consider the velocity profile of a number of clearly defined iCMEs and the relationship between iCME velocities and that of the background solar wind. The results provide additional confirmation that iCMEs converge towards the velocity of the solar wind ahead of the event and that most of the resulting acceleration or deceleration occurs in the innermost regions of the solar wind.

1. Introduction

Coronal Mass Ejections (CMEs) are spectacular events in which large amounts of material are ejected into the solar wind from the corona and chromosphere, becoming visible to white-light instruments as they pass out through the corona. CMEs were first identified by space-borne coronagraphs in the 1970s and were quickly observed to be a common occurrence of solar activity [*Tousey et al.*, 1973; *MacQueen et al.*, 1974; *Gosling*, 1999]. The launch of the Solar and Heliospheric Observatory (SoHO) [*Domingo et al.*, 1995] spacecraft in 1996 and improved sensitivity of the Large-Angle and Spectrometric Coronagraph (LASCO) aboard led to the detection of a much larger number of CMEs than expected, with the variation in CME structure being much greater than originally expected. A detailed list of LASCO CME events can be found at (http://lasco-www.nrl.navy.mil/cmelist.html).

If there is a large difference in velocity between the CME and that of the background solar wind a shock may develop at the boundaries which will produce particle acceleration, resulting in radio emission. Radio bursts produced in this way have been used by *Gopalswamy et al.* [2000] to track iCMEs through interplanetary space. Their results showed that the velocity profile of a iCME is heavily dependent on the initial velocity of the CME. Slow CMEs below 400 km s^{-1} are observed to increase in velocity as the iCME moves out from the Sun. Fast CMEs, those with a velocity above 400 km s^{-1}, are observed to decrease in velocity as the iCME moves out into interplanetary space.

The slow solar wind in the ecliptic plane has typical velocities in the region of 300-400 kms^{-1}, so the results in [*Gopalswamy et al.*, 2000] are consistent with CMEs emerging into regions dominated by slow solar wind and converging onto the background solar wind speed. The purpose of this paper is to use the ability of IPS to measure both the iCME speed and solar wind speed ahead of the event to confirm this. **Figure 1.**

The classical picture for a CME consists (since the pre SOHO era) of a three part structure [*Hundhausen et al.*, 1984], with a front, void and dense core. The front is the leading edge of the CME and encloses the void, which is an area devoid of material when compared with the dense core (commonly prominence material) which follows it. The term "iCME" used in this paper refers to structures seen in IPS observations associated with coronal eruptions seen in white-light observations.

In this study we have considered CMEs that appear to have a well defined three part structure in the corona and have assumed that the iCME has expanded radially out from the Sun and was rotationally symmetrical. iCMEs are known to expand preferentially into regions of dominantly fast wind [*Gosling et al.*, 1994] and their shape may be distorted with interaction with other structures such as stream interfaces. These effects are likely to be less well-developed in the inner regions of the solar wind. Modelling the CME as a "blob" is justified as a first approximation as the evolution of a CME in interplanetary space is still an unknown. However, if the observed enhancement in scintillation comes from the CME core (as suggested by some of the observations discussed in section 3) it should be possible to assume to a reasonable degree of accuracy that it has the form of a uniform spherical expanding blob.

2. Interplanetary Scintillation (IPS)

Interplanetary scintillation observations of the solar wind have been made for more than forty years [*Hewish and Wills*, 1964; *Dennison and Hewish*, 1967]. Originally IPS measurements were taken using a single antenna, but developments in the field led to observations using two widely spaced antenna to measure the scintillation pattern [*Armstrong and Coles*, 1972]. An estimate of solar wind speed can be obtained from the time lag for maximum correlation, provided that the IPS observations are made when the ray paths from the radio source to the antennas lie in a plane which passes through the centre of the Sun, as shown in Figure 2 [*Bourgois et al.*, 1985; *Coles et al.*, 1995]. **Figure 2.**

The accuracy to which IPS can determine solar wind speed improves as the baseline projected into the plane of sky between the antennas increases (B_{par} in Figure 2). The time lag for maximum correlation also increases, and as this happens the ability to resolve the different solar wind speeds across the ray path improves [*Grall*, 1995; *Rao et al.*, 1995; *Breen et al.*, 2006]. However, the irregularity pattern giving rise to IPS will be evolving with time, so the maximum correlation between the two scintillation patterns observed by the sites decreases as the parallel baseline increases [*Moran*, 1998].

All of the data used in this paper were taken using the EISCAT UHF system, which was originally constructed as an ionospheric radar system [*Rishbeth and Williams*, 1985]. Its high timing accuracy, low noise receivers and long baselines make it a powerful tool for IPS observations [*Bourgois et al.*, 1985; *Breen et al.*, 1996b, c].

2.1. iCME characteristics in IPS observations

EISCAT has observed mass ejections from the Sun since the start of regular observations in the early 1990s. Work by *Grall* [1995] and *Klinglesmith* [1997] showed that an iCME passing through the ray path of two sites would cause identifiable signatures in the IPS cross-correlation functions. *Grall et al.* [1996] and *Klinglesmith* [1997] observed a magnetic field rotation caused by the passage of an iCME through the IPS ray path. However, consideration of iCMEs in long baseline observations remained at the case study level until *Canals* [2002] who proposed a set of four IPS signatures when an iCME was present in an IPS observation.

CMEs have been identified using both white-light coronagraph images of the corona and in-situ magnetic and plasma data from spacecraft in interplanetary space. These sets of observations have very different signatures for a CME but can be related to one another.

White-light observations of a CME show that these dense structures evolve over time-scales of hours to days [*Sheeley et al.*, 1997], compared with the slower changes over several days arising from rotation of quasi-static structures (e.g. streamers) observed in the field of view. In-situ observations of iCMEs indicate a rotation of the magnetic field when viewed from a single location in space as the iCME passes over the specific location, while in-situ measurements of counter-streaming electrons propagating along the field lines of the iCME are consistent with the iCME field lines either being attached to the Sun or forming a closed magnetic loop.

Both white-light and in-situ observations have their counterparts in IPS observations [*Klinglesmith*, 1997; *Lynch et al.*, 2002]. The IPS signatures of an iCME passing through the ray-path used in this study were proposed by *Canals* [2002]:

1. A significant variation in the intensity of scintillation on time-scales of 10s of minutes to 10s of hours (*corresponds to a dense structure moving through the ray-path*);

2. significant variation in the form of the cross-correlation function, and cross spectra of the scintillation patterns detected at the receiver sites, with the changes taking place on timescales of 10s of minutes to 10s of hours (*corresponds to the change*

in the distribution of electron density along the IPS raypath as a dense transient structure passes through it);

3. the presence of a clearly defined negative lobe in the cross-correlation function near zero time-lag (*corresponds to rotation of the magnetic field e.g. [Klinglesmith, 1997; Breen et al., 1997; Lynch et al., 2002]*);

4. the results of fitting the observed data required that the modelled irregularities producing the scintillation be elongated perpendicular to the direction of the bulk flow (*corresponds to rotation of the magnetic field*).

These signatures in IPS measurements indicate whether or not an iCME is likely to occupy some portion of the ray path, and the more signatures that an observation shows the greater the likelihood that it included an iCME. These four signatures relate to different features of the iCME. Signatures 1 and 2 correspond to the observed dense transient features seen in white light coronagraphs passing through the line of sight. Signatures 1 and 2 both indicate more rapid change than would be produced by the rotation of quasi-static features (co-rotating interaction regions or slow flow above streamers) through the field of view. Signature 3 is associated with a significant rotation in the magnetic field from the radial direction [*Grall*, 1995], this in turn rotates the density irregularities giving rise to IPS. As the density irregularities themselves are anisotropic [*Grall et al.*, 1997], the scale size of the spatial correlation function along the major axis grows in a way which is roughly proportional to the axial ratio of the irregularities. The width perpendicular to the major axis shrinks slightly, but stays roughly fixed at the Fresnel scale [*Klinglesmith*, 1997]. If the irregularities, and consequently the spatial correlation functions are isotropic, then the function has a negative side lobe running symmetrically around the central peak. As the anisotropy increases, this negative side lobe increases in depth and becomes re-arranged so that it is symmetrical about the major axis, and the correlation function remains positive along the major axis. Provided that the major axis is close to parallel to the outflow direction (and thus perpendicular to the IPS ray-path at the P-point), the correlation function remains positive at zero-lag. However, if the magnetic field direction is rotated so that the irregularities are elongated perpendicular to the outflow direction (and thus close to parallel to the IPS ray-path), then the zero-lag point of the temporal cross-correlation function will sample the negative lobe of the cross-correlation function [*Klinglesmith*, 1997]. This will give rise to clear negative cross-correlation at zero-lag, as seen in Figure 7. The fourth signature is also caused by the magnetic field rotation when a iCME passes through the ray path, it rotates the irregularities which give rise to interplanetary scintillation and is described in detail in *Klinglesmith* [1997], *Canals* [2002] and *Lynch et al.* [2002].

3. Linking white-light CME observations with IPS observations of interplanetary transients

The white-light LASCO CME list was first used to find cases where the chances of a CME passing through the ray path during an observation were high. This was done following the method listed below:

1 The CME was mapped out from the Sun using the LASCO plane of sky velocity;

2 if the arrival time of CME was within ± 5 hours of the IPS observation, then the observation was selected for further investigation;

3 if the IPS observations after an initial fitting showed one of more iCME signatures

passing through the ray path, these were selected for further investigations. The more iCME signatures that a IPS observations had, the more likely that an iCME was present in the ray path.

If any IPS observations showed two or more characteristics of iCME activity they were taken on to be analysed further. Several assumptions have to be made for the fitting of the IPS observation. These were:

1. That the CME is rotationally symmetrical about its central axis;
2. the longitude of origin can be estimated from coronal dimming seen in EIT 195Å observations. We did this using EIT 195Å difference images from ;
3. the angular extent of the event was estimated from LASCO images.

Using these assumptions the fitting and eventual comparison between the CME velocity and the background solar wind can be preformed. The fitting analysis of the IPS observations followed the same method for each CME candidate. EIT 195Å observation were used to detect dimming regions because their high cadence increased the chances of observing the regions of depleted plasma following a CME.

Stage 1 Observations were fitted making the assumption that solar wind structure was that of the undisturbed background solar wind. IPS observations were constrained by using white-light maps of solar activity and relating the position of the IPS ray-path to quasi-static coronal structures [e.g. *Breen et al.*, 1996b].

Stage 2 Scintillation from the CME was assumed to overwhelmingly dominate the observation so that the contribution of the background solar wind to the observation is insignificant. This was equivalent to assuming that the iCME occupied the whole ray path.

Figure 3.

Stage 3 The iCME was modelled as a uniform expanding blob. EIT 195 Å dimming images were used to estimate the longitude of origin of the CME and then the plane of sky velocity obtained from LASCO was corrected for the cosθ effect to give a radial velocity. The iCMEs were then mapped out to the IPS ray path at the radial velocity along the appropriate spiral for the iCME velocity. **Figure 4.**

In the mapping it is recognised that the (i)CME material expands from the Sun approximately radially, but that the overall magnetic structure of the event will become draped in longitude in a spiral by the rotation of the Sun (e.g. *Cane et al.* [1988] cited in *Cane* [1999]).

The information obtained from stages 1-3 enabled a comparison of the observational auto- and cross-spectra with the results of a 2-dimensional weak scattering fitting programme developed at University of San Diego, California [*Grall*, 1995; *Coles*, 1996; *Klinglesmith*, 1997; *Massey*, 1998] to provide an estimate of velocity for the iCME. The programme was originally applied to CMEs by *Lynch et al.* [2002]. The model was constrained by using the assumptions described in stages 1-3. Quality of fit was undertaken by comparing the χ_{ν}^{2} values for each fit, the aim being to obtain a χ_{ν}^{2} as close to 1 as possible [e.g. *Reiff*, 1983]. If the value of χ_{ν}^{2} closest to 1 was obtained with the assumptions in stage 1, then no further fitting was undertaken as this suggested that no iCME was present in the observation. In cases where fitting suggested iCMEs were present (best fit with assumptions 2 or 3), the estimated iCME velocity was compared with background solar wind velocity determined by fitting observations of the same source on previous days, or sources further out along the likely iCME path on the same day. These fits were constrained by the use of Carrington white-light maps [e.g. *Breen et al.*, 1996b].

Analysing the data in this way made it possible to compare the iCME velocity with solar wind velocities in the same region of space from pervious days or further out along the same streamline of flow.

3.1. Observations

The IPS observations were taken between 1997 and 2005. The majority of the observations used in this paper are taken using the EISCAT [*Rishbeth and Williams*, 1985; *Breen et al.*, 1996b] system but there is one iCME observation where both EISCAT and MERLIN [*Thomasson*, 1986; *Breen et al.*, 2000b] were combined [*Bisi et al.*, 2005].

3.1.1. Multi Element Radio Linked Interferometer Network (MERLIN)

MERLIN is an array of radio telescopes located at several different locations around the UK. The control site is at Jodrell Bank, with telescopes at Cambridge, Defford, Knockin, Wardle, Darnhall and Tabley. The observations discussed in this paper were taken using the Jodrell Bank, Cambridge and Knockin telescopes. The MERLIN IPS measurements can be made at 5 GHz and 1.4 GHz.

3.1.2. European Incoherent Scatter Radar (EISCAT)

The EISCAT system, consists of three antennas at Tromsø in Norway, Kiruna in Sweden and Sodankylä in Finland plus two antennas on the island of Svalbard. Most of the observations discussed in this paper used the Tromsø, Kiruna and Sodankylä telescopes receiving at a central frequency of 928 MHz , which allowed weak scattering observations of the solar wind from approximately 20R_s to more than 100R_s. More recently EISCAT has been fitted with a secondary receiving system operating at a central frequency of 1400 MHz and extending the weak scattering regime closer to the Sun [*Wannberg*, 2002]. This capability was used for the combined EISCAT-MERLIN observation.

Using the criteria described in section 3, there were 168 CMEs that could have crossed the IPS ray-path during an observation. 43 of these showed two or more iCME characteristics. These 43 cases were analysed further and it was found that there were 7 cases where IPS observations showing iCME characteristics could be linked to a LASCO CME.

4. Results

4.1. Case study

The observation of source 1150-003 on the 29th September 1997 was a series of 15 minute observations made every hour for 4 hours. The IPS observation was linked to a CME on the 28th September 1997. The CME consisted of several different features, listed in Table 1.

Figure 5.

The eruption site of CME was at Position Angle (PA) 257 (position in degrees taken anticlockwise from the north pole of the sun) and the event had an approximate width of 40°. The velocity of the different white-light features of interest were calculated on an individual basis and are listed in Table 1.

Figure 6.

Table 1.

The IPS observations showed clear signatures of CME activity. These included a significant variation in the cross correlation functions and scintillation levels between the different 15 minute observations, with a maximum in scintillation occurring at 1001 UT. The cross correlation function showed a clear negative lobe, strongly indicative of an iCME at the zero time lag point during the 1001 UT observation. This feature was not present during the other observations. **Figure 7.**

The data from this case study indicated that the iCME passed through the IPS line of sight before the start of the series of observations at 1001 UT. Using the velocity of the different features from Table 1 it could be estimated when different features were likely to cross ray path. These features were mapped out using their plane of sky velocities to the IPS distance. **Table 2.**

From Table 1 it can be seen that several different internal features of the iCME could have caused the IPS observation. The most probable candidate for the IPS observation were the arcades (Table 1, third entry), but the possibility of interaction with other internal features of the same iCME is highly likely.

The interaction between different internal structures of the iCME may have caused a "self-cannibalisation" effect whereby the IPS signatures were probably caused by a combination of more than one of the features of the iCME. This is supported by the velocities obtained from the C2, and C3 coronagraphs and IPS observations. The white-light velocities imply a deceleration of the CME as it moves through the coronagraphs fields of view. The IPS velocity is slightly higher than the C3 velocity which could indicate an acceleration of the material between the C3 and IPS distances. This variation in the velocity profiles could be explained by the last fronts which were travelling at a higher velocity and so overtook and interacted with the arcades in front.

The IPS velocity of the iCME was not significantly different from the background solar wind speed therefore indicating that the majority of the iCME acceleration took place quite close to the Sun. Unfortunately due to the overall intricacy of this event it is extremely difficult to state with certainty which section of the iCME caused the IPS observation. This event would not have been preceded by a shock front as its speed was close to that of the solar wind.

4.2. IPS observations of iCMEs

Six more iCME events are listed in Table 3. The velocity profiles of the different iCMEs and that of the solar wind ahead of each event can also be seen in Table 4. **Table 3.** **Table 4.**

Table 4 provides information on the variation in the velocity between the white-light event and the IPS observation. For the majority of cases the iCME speed as it crosses the IPS line-of-sight is close to that of the background solar wind. We suggest this is due to the interaction between the iCME and the background solar wind.

The observations have shown several different velocity profiles for CMEs which in general follow the rule that a CMEs with a velocity less than that of the background solar wind have been accelerated and CMEs with velocities greater than that of the background solar wind have been decelerated to some extent. Case 3 is anomalous but may represent a late-decelerating event of the type reported in [*Tappin*, 2006]. Observations where in-situ measurements are available show that by the time the iCME has reached the spacecraft the iCME speed is little changed from the speed determined from the IPS result.

5. Discussion

The velocities of the iCMEs when they cross the line of sight are, in most cases, comparable to that of the background solar wind as shown in Table 4. This suggests that the deceleration of the iCMEs is a very rapid process and is almost complete by the IPS distances.

The IPS observations of iCMEs point towards IPS observations being sensitive to fainter CMEs when compared with LASCO and the Solar Mass Ejection Imager (SMEI) white light instruments. Faint events are more frequent so an instrument which observes intermittently (like EISCAT) is more likely to see them, whereas LASCO and SMEI observe near continuously but are more likely to detect stronger events. This could be caused by the IPS sensitivity to electron density which is approximately N_e^2 whereas white light instruments are sensitive approximately to N_e (electron density), so small differences in the electron density are more clearly seen in IPS observations. EISCAT observations are thus more likely to be detecting the slower and weaker event, whereas the white light instruments of LASCO and the Solar Mass Ejection Imager (SMEI) [*Eyles et al.*, 2003] are more sensitive to the larger events [*Tappin*, 2006] which are faster and pick up more material on their leading edge. Events which stayed faster than the solar wind to greater distances from the Sun would pick up more material and so might be more likely to be detected by SMEI (Tappin, private communication, 2006).

Counter-streaming electrons propagating around a closed loop or magnetic field lines still attached to the Sun have been identified as an in-situ characteristic of an iCME by several different instruments. It is possible such a field configuration would give rise to large rms_{perp} values appearing when IPS data is fitted by MHD waves propagating along field lines. At present this is only a tentative suggestion, but further investigation may be profitable.

6. Conclusions

We now have a reliable method of associating iCMEs seen in IPS observations as interplanetary extensions of CMEs seen in the corona. The ability of IPS to provide velocity measurements for the background solar wind has been invaluable in this study. Comparisons of CME speeds in the corona with those of iCME speeds in interplanetary space and of the background solar wind ahead of the event clearly show the iCME converges onto the background solar wind speed, with most of the acceleration taking place in the inner region of the solar wind. **Figure 8.**

The results show that the background solar wind has a significant effect on the velocity profile of an iCME. The internal structure of an iCME may also have an effect on the observed velocity as different phases of the event interact with one another as the iCME travels through interplanetary space. These observations show that CME evolution and propagation is a complex problem, where the different internal structures that make up a CME can interact with one another. It is reasonable to assume that this "self-cannibalisation" regularly takes place inside of iCMEs as they propagate through interplanetary space.

The launch of the Heliospheric imager [*Harrison et al.*, 2005] instruments on the Solar TErrestrial RElations Observatory (STEREO) should greatly assist understanding of the interaction between different iCMEs, their evolving internal structure and their interaction with the background solar wind.

Our understanding of the evolution of CMEs should be greatly improved by 3D imaging of these events as they propagate away from the Sun, revealing how the internal makeup of these events alters as a CME moves out from the Sun and interacts with the solar wind. As the fields of view overlap STEREO will also be able to provide information on which feature in the CME is causing the changes in scintillation in IPS observations. STEREO data will also provide better information on the location of regions of enhanced density in the IPS ray path, reducing the uncertainties in IPS analysis. However, it is likely that particularly far from the Sun STEREO may not be able to resolve faint iCMEs. Co-ordinated programmes of white-light, IPS, radio burst and in-situ measurements will be required to fully understand CME evolution and their interaction with the background solar wind. The upcoming International Heliophysical year provides the ideal framework for these studies.

Acknowledgments. We wish to thank the director and staff of EISCAT for the use of the EISCAT IPS data used in this study. EISCAT is supported by the scientific research councils of Finland, France, Germany, Japan, Norway, Sweden and the UK. We made use of the LASCO CME catalogue in the course of this study. This CME catalogue is generated and maintained by the Center for Solar Physics and Space Weather, The Catholic University of America in co-operation with the Naval Research Laboratory and NASA. The LASCO white-light data were made available by the LASCO consortium. SoHO is a project of international co-operation between ESA and NASA. The IPS analysis routines used in this study were developed at University of California, San Diego and we would like to thank W.A. Coles for making them available to us. Three of us (RAJ, RAF and MMB) were supported by PPARC during the period when this work was carried out. The University of Wales, Aberystwyth, funded AC.

References

Armstrong, J. W., and W. A. Coles (1972), Analysis of three-station interplanetary scintillation data, *J.Geophys.Res.*, *77*, 4602–4610.

Bisi, M. M., A. R. Breen, R. A. Fallows, and et al. (2005), Combined EISCAT/ESR/MERLIN Interplanetary Scintillation Observations of the Solar Wind, in *ESA SP-592: Solar Wind 11/SOHO 16, Connecting Sun and Heliosphere*.

Bourgois, G., W. A. Coles, G. Daigne, J. Silen, T. Turunen, and P. J. Williams (1985), Measurements of the solar wind velocity with EISCAT., *Astronomy and Astrophysics*, *144*, 452–462.

Breen, A., P. Moran, C. A. Varley, W. Wilkinson, P. J. S. Williams, W. A. Coles, R. Grall, T. Klingesmith, and J. Makkanen (1997), EISCAT Measurements of the Solar Wind: Observations of Interaction Regions , *Phys. Chem. Earth*, p. 387.

Breen, A. R., W. A. Coles, R. Grall, U.-P.L_vhaug, J. Markkanen, H. Misawa, and P. J. S. Williams (1996b), EISCAT measurements of interplanetary scintillation, *Journal of Atmospheric and Terrestrial Physics*, *58*, 507–519.

Breen, A. R., W. A. Coles, R. R. Grall, M. T. Klinglesmith, J. Markkanen, P. J. Moran, B. Tegid, and P. J. S. Williams (1996c), EISCAT measurements of the solar wind, *Ann. Geophysicae*, *14*, 1235–1245.

Breen, A. R., S. J. Tappin, C. A. Jorden, P. Thomasson, P. J. Moran, R. A. Fallows, A. Canals, and P. J. S. Williams (2000b), Simultaneous interplanetary Scintillation and Optical measurements of the acceleration of the Slow Solar Wind., *Annales Geophysicae*, *18*, 995–1002.

Breen, A. R., A. Canals, R. A. Fallows, P. J. Moran, and M. Kojima (2002a), Large-scale structure of the solar wind from interplanetary scintillation measurements during the rising phase of cycle 23, *Advances in Space Research*, *29*, 379–388.

Breen, A. R., R. A. Fallows, M. M. Bisi, P. Thomasson, C. A. Jordan, G. Wannberg, and R. A. Jones (2006), Extremely long-baseline Interplanetary Scintillation measurements of Solar Wind velocity, *Journal of Geophysical Research*, in press.

Canals, A. (2002), Interplanetary Scintillation Studies of the Solar Wind during the Rising Phase of the Solar Cycle., Ph.D. thesis, University of Wales, Aberystwyth.

Cane, H. (1999), The current status in our understanding of energetic particle, coronal mass ejections, and flares, in *Coronal Mass Ejections*, edited by N. Crooker, J. A. Joselyn, and J. Feynman, Geophysical Monograph Series, pp. 205–216, American Geophysical Union, including IUGG Volumes, Maurice Ewing Volumes, and Mineral Physics Volumes.

Cane, H. V., D. V. Reames, and T. T. von Rosenvinge (1988), The role of interplanetary shocks in the longitude distribution of solar energetic particles, *Journal of Geophysical Research*, *93*, 9555–9567.

Coles, W. A. (1996), A Bimodal Model of the Solar Wind Speed, *Astrophys. Space sci*, *243*, 87–+.

Coles, W. A., R. Grall, T. Klinglesmith, and G. Bourgois (1995), Solar Cycle changes in the level of compressive mircoturbulance near the Sun, *Geophysical Research*.

Dennison, P., and A. Hewish (1967), The solar wind outside of the plane of the ecliptic, *Nature*.

Domingo, V., B. Fleck, and A. I. Poland (1995), SOHO: The Solar and Heliospheric Observatory, *Space Science Reviews*, *72*, 81–+.

Eyles, C. J., et al. (2003), The Solar Mass Ejection Imager (Smei), *Solar physics*, *217*, 319–347.

Gopalswamy, N., A. Lara, R. P. Lepping, M. L. Kaiser, D. Berdichevsky, and O. C. St. Cyr

(2000), Interplanetary Acceleration of Coronal Mass Ejections, *Geophysical Research Letters*, *27*, 145–148.

Gosling, J. T. (1999), Coronal Mass Ejections: An overview, *Geophysical Monograph 99-Coronal Mass Ejections*, pp. 9–16.

Gosling, J. T., S. J. Bame, D. J. McComas, J. L. Phillips, B. E. Goldstein, and M. Neugebauer (1994), The speeds of coronal mass ejections in the solar wind at mid heliographic latitudes: Ulysses., *Geophysical Research letters*, *21*, 1109–1112.

Grall, R. R. (1995), Remote Sensing Observations of the Solar Wind Near the Sun., Ph.D. thesis, University of California, San Diego.

Grall, R. R., W. A. Coles, M. T. Klingesmith, A. R. Breen, P. J. S. Williams, J. Markkanen, and R. Esser (1996), Rapid acceleration of the polar solar wind, *Nature*.

Grall, R. R., W. A. Coles, S. R. Spangler, T. Sakurai, and J. K. Harmon (1997), Observations of field-aligned density microstructure near the Sun, *Journal of Geophysical Research*, *102*, 263–274, doi:10.1029/96JA03142.

Harrison, R., C. Davis, and C. Eyles (2005), The STEREO Heliospheric Imager: How to detect CMEs inthe heliosphere, *Adv Space Research*, *36*.

Hewish, A., and S. D. Wills (1964), Interplantary scintillations of small diameter radio sources, *Nature*, *203*, 1214.

Hundhausen, A. J., C. B. Sawyer, L. House, R. M. E. Illing, and W. J. Wagner (1984), Coronal mass ejections observed during the solar maximum mission - Latitude distribution and rate of occurrence, *Journal of Geophysical Research*, *89*, 2639–2646.

Klinglesmith, M. (1997), The polar solar wind from 2.5 to 40 solar radii: Results of intensity scintillation measurements, *Ph.D. Thesis*.

Lynch, B. J., W. A. Coles, and N. R. Sheeley (2002), A comparison of mean density and microscale density fluctuations in a CME at 10 R_{solar}, *Geophysical research letters*, *29*, 19–1.

MacQueen, R. M., J. A. Eddy, J. T. Gosling, E. Hildner, R. H. Munro, G. A. Newkirk, A. I. Poland, and C. L. Ross (1974), The Outer Solar Corona as Observed from Skylab: Preliminary Results, *Astrophys. J. Lett*, *187*, L85+.

Massey, W. (1998), Measuring Intensity Scintillations at the Very Long Baseline Array (VLBA) to Probe the solar Wind.

Moran, P. J. (1998), Interplanetary scintillation measurements of the solar wind using EISCAT, Ph.D. thesis, University of Wales, Aberystwyth.

Rao, A. P., S. Ananthakrishnan, V. Balasubramanian, and W. A. Coles (1995), Very long baseline IPS observations of the solar wind speed in the fast polar streams, in *Solar Wind Conference*, pp. 94–+.

Reiff, P. H. (1983), The Use and Misuse of Statistical Analyses, in *ASSL Vol. 104: Solar-Terrestrial Physics: Principles and Theoretical Foundations*, edited by R. L. Carovillano and J. M. Forbes, pp. 493–+.

Rishbeth, H., and P. J. Williams (1985), The EISCAT Ionspheric Radar:the system and its Early Results., *Q. Jl R. astr. Soc.*, *26*, 478–512.

Sheeley, N. R., Jr., et al. (1997), Measurements of Flow Speeds in the Corona between 2 and 30 R sub sun, *Astrophysical Journal*, *484*, 472–+, doi:10.1086/304338.

Tappin, S. J. (2006), The Deceleration of an Interplanetary Transient from the Sun to 5 Au, *solar physics*, *233*, 233–248, doi:10.1007/s11207-006-2065-2.

Thomasson, P. (1986), MERLIN, *Royal Astronomical Society, Quarterly Journal*, *27*, 413–431.

Tousey, R., J. D. F. Bartoe, J. D. Bohlin, G. E. Brueckner, J. D. Purcell, V. E. Scherrer, N. R.

Sheeley, R. J. Schumacher, and M. E. Vanhoosier (1973), A Preliminary Study of the Extreme Ultraviolet Spectroheliograms from Skylab, *Solar Physics*, *33*, 265–+.

Wannberg, G. (2002), The new 1420 MHz dual-polarisation interplanetary scintillation (IPS) facility at EISCAT, Proc. Union of Radio Scientists (URSI) 2002.

R. A. Jones, Institute of Mathematical and Physical Sciences, University of Wales, Aberystwyth, SY23 3BZ, UK (raj98@aber.ac.uk)

Received ________________________

This manuscript was prepared with AGU's LaTeX macros v5, with the extension package 'AGU^{++}' by P. W. Daly, version 1.6b from 1999/08/19.

Figure Captions

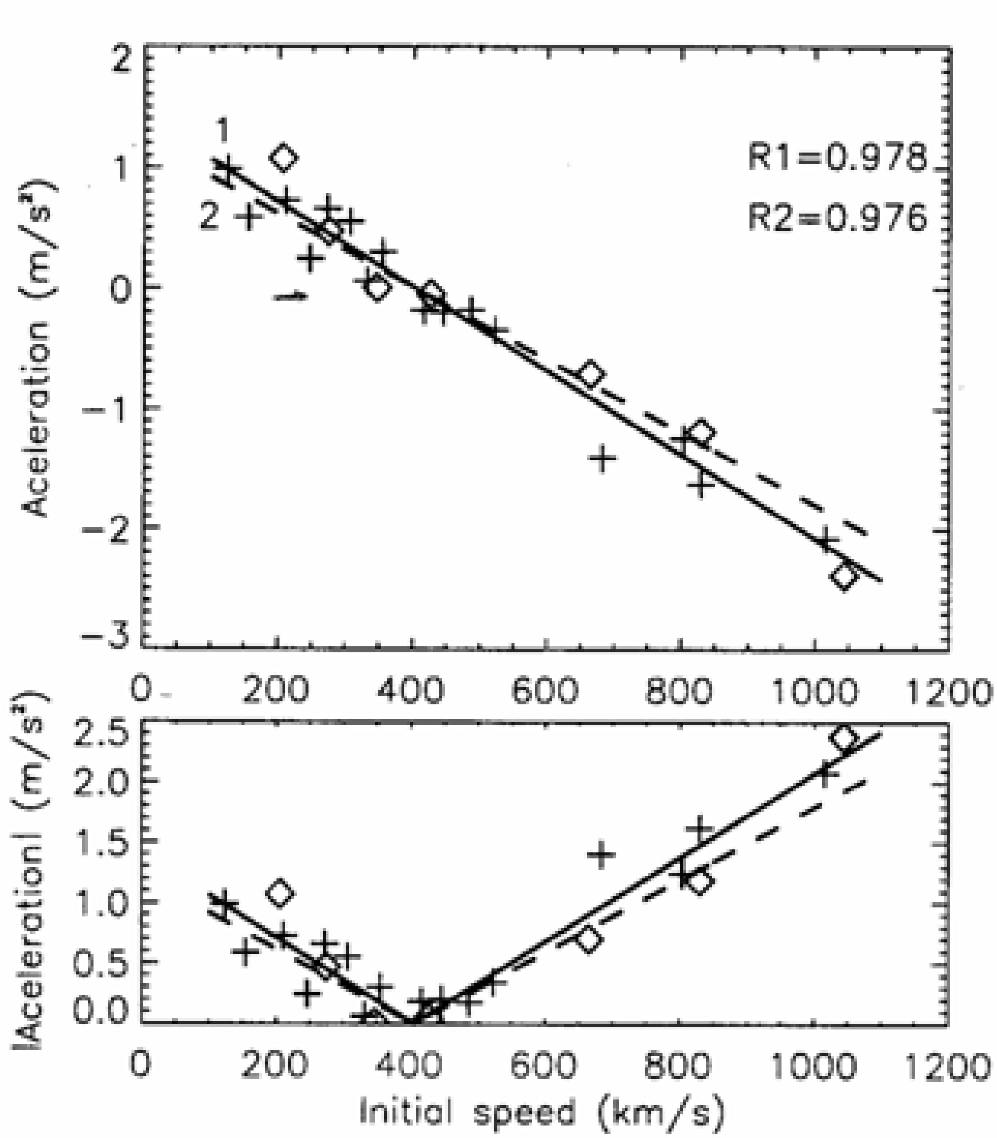

Figure 1. The acceleration and initial velocity profiles of several different iCMEs from *Gopalswamy et al.* [2000].

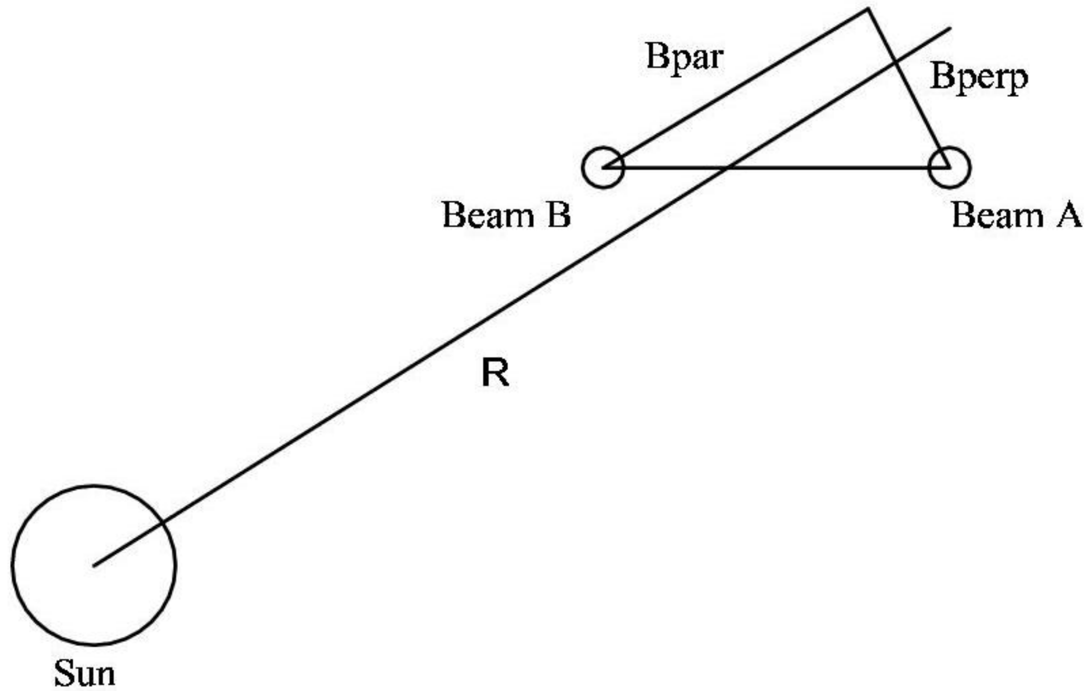

Figure 2. Two station observation of interplanetary scintillation, viewed from the radio source [*Breen et al.*, 2002a]. Maximum correlation between the two antenna occurs when the baseline between the two sites is parallel to the outflow direction of the solar wind across the ray path, with the time lag determined by drift velocity of the scintillation pattern between the two antennas [*Moran*, 1998]. The radial and tangential baselines to the Sun-Earth direction in the plane of the sky are shown as B_{par} and B_{perp} respectively.

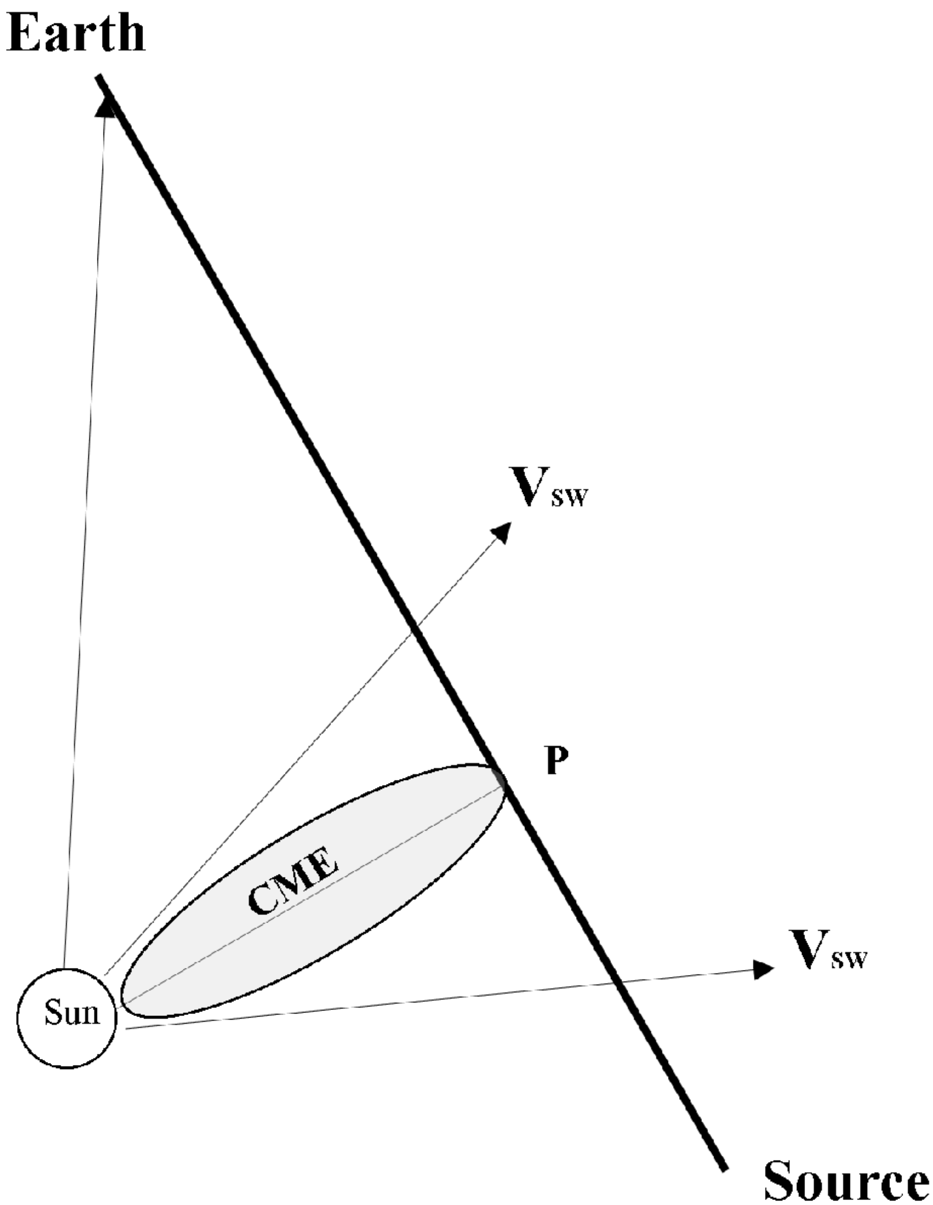

Figure 3. CME is assumed to dominate entire ray path and is modelled as such

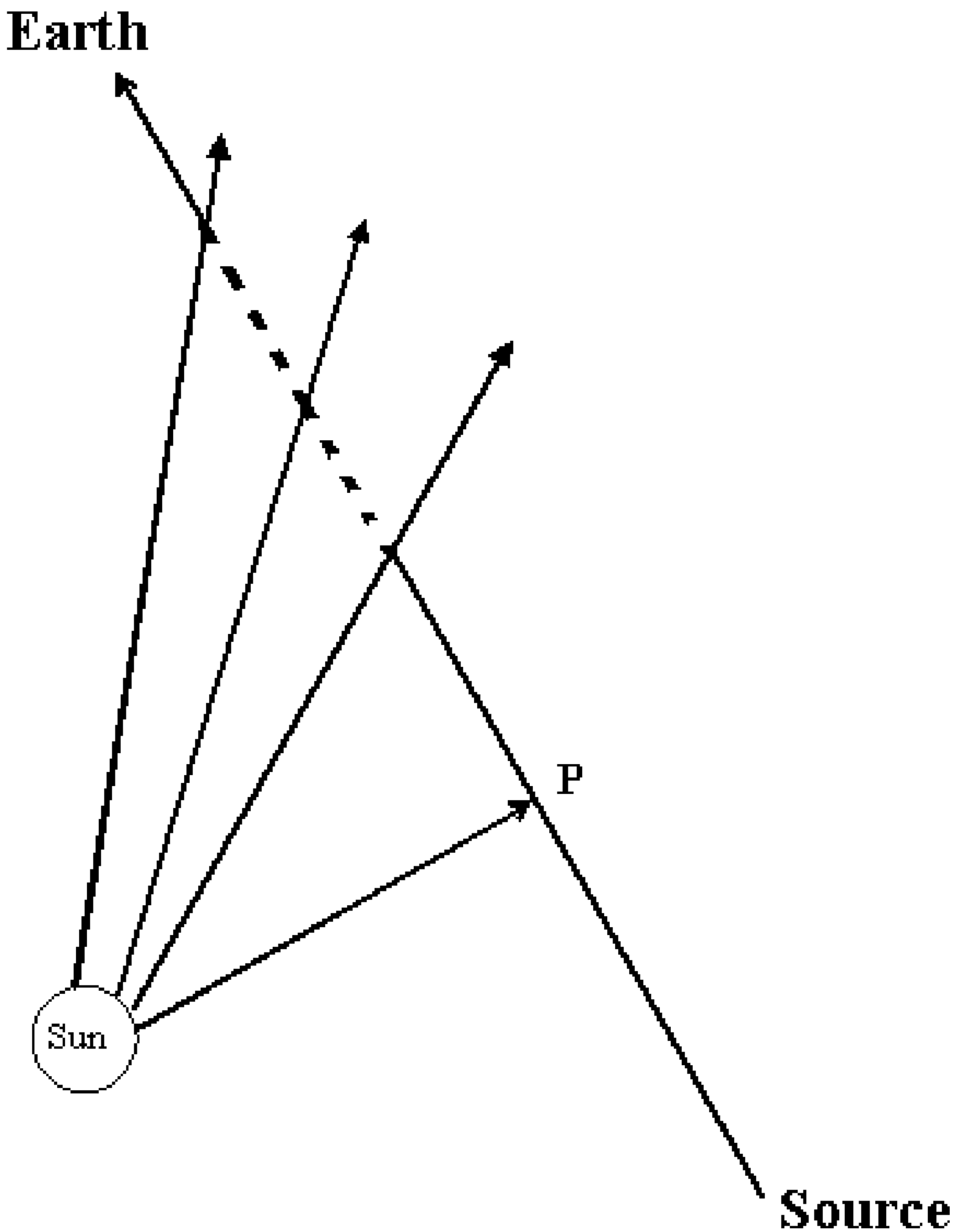

Figure 4. CME is modelled as an expanding blob in the IPS ray path which the dashed line denotes.

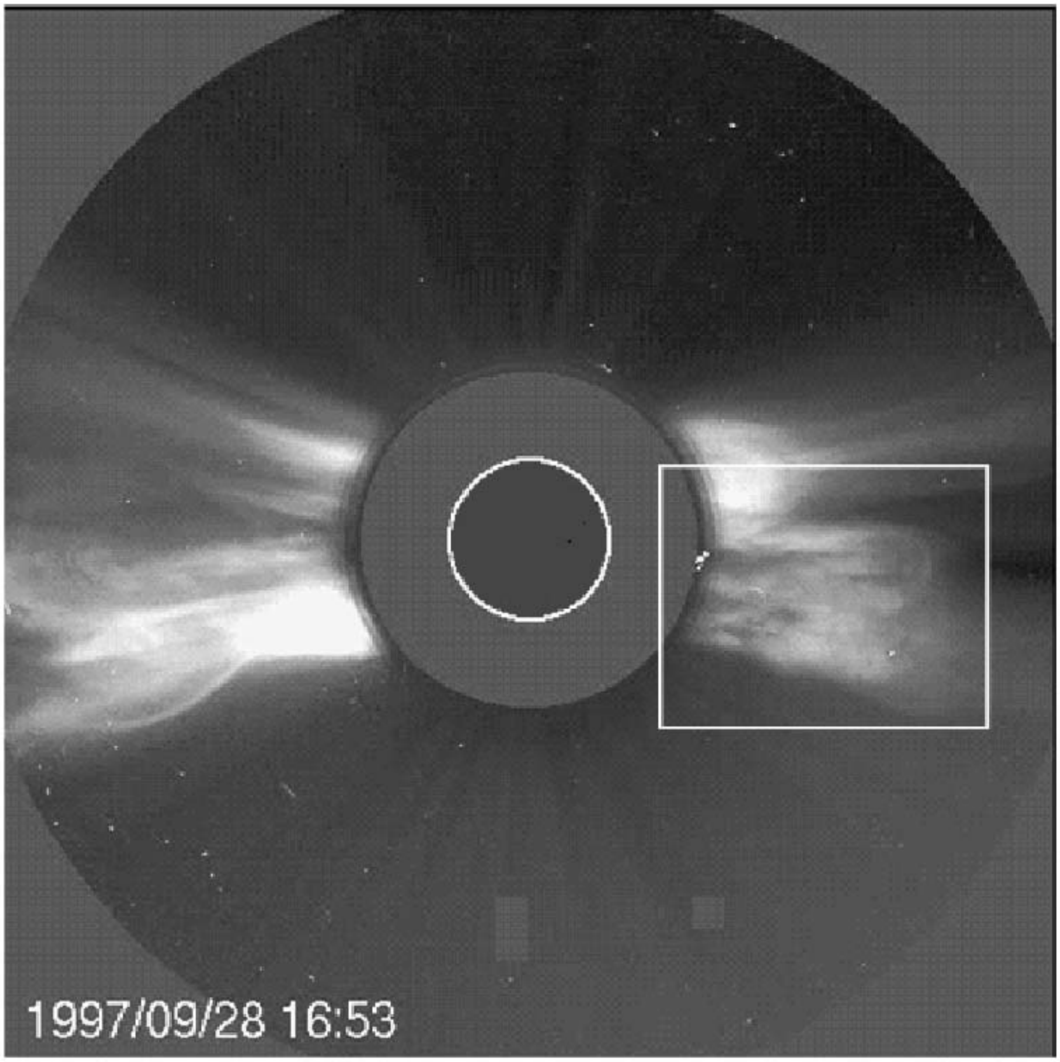

Figure 5. LASCO C2 image of a CME eruption on the 28th September 1997.

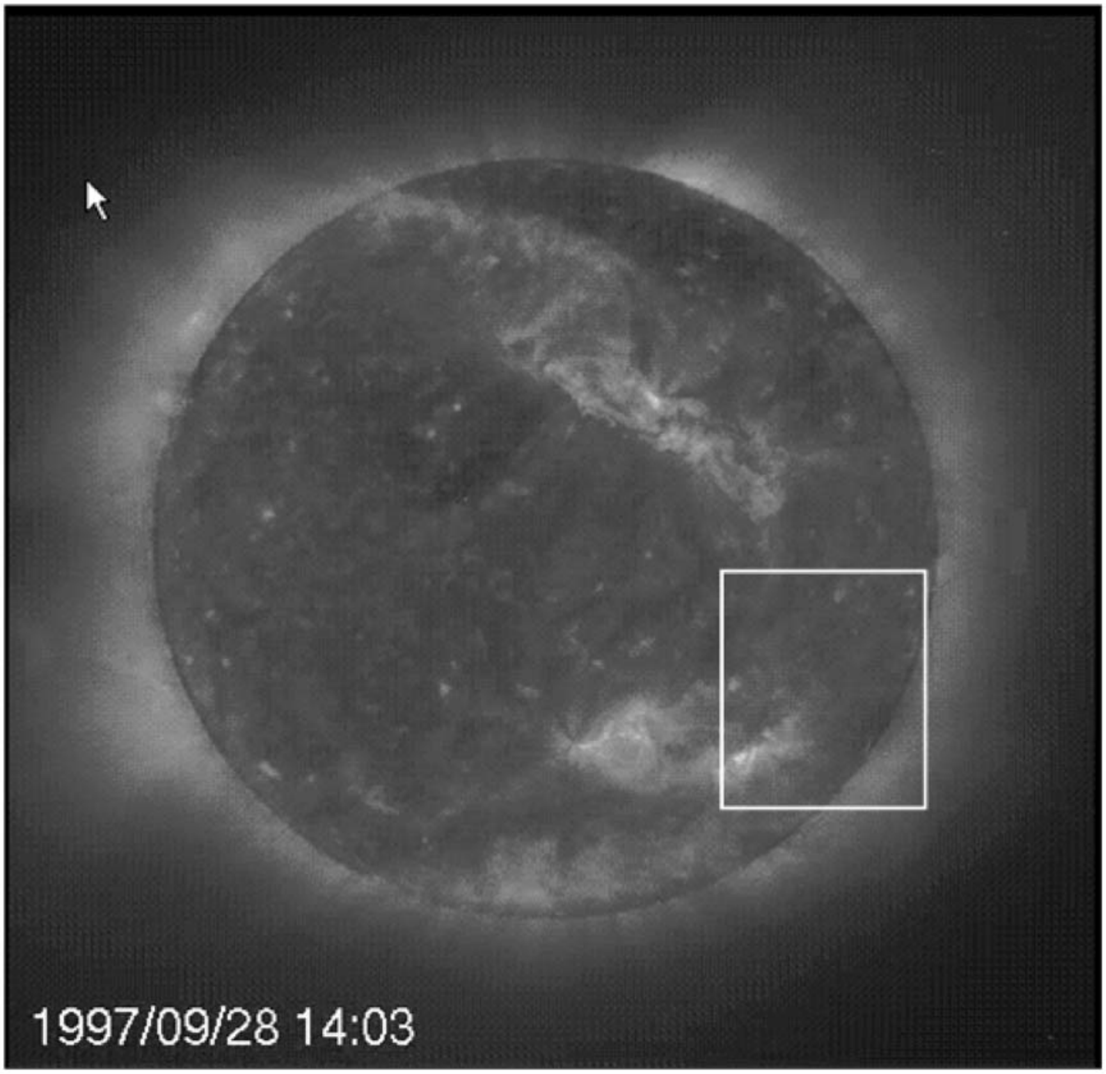

Figure 6. EIT 195 Å image of the eruption site for the CME observed on the 28th September 1997.

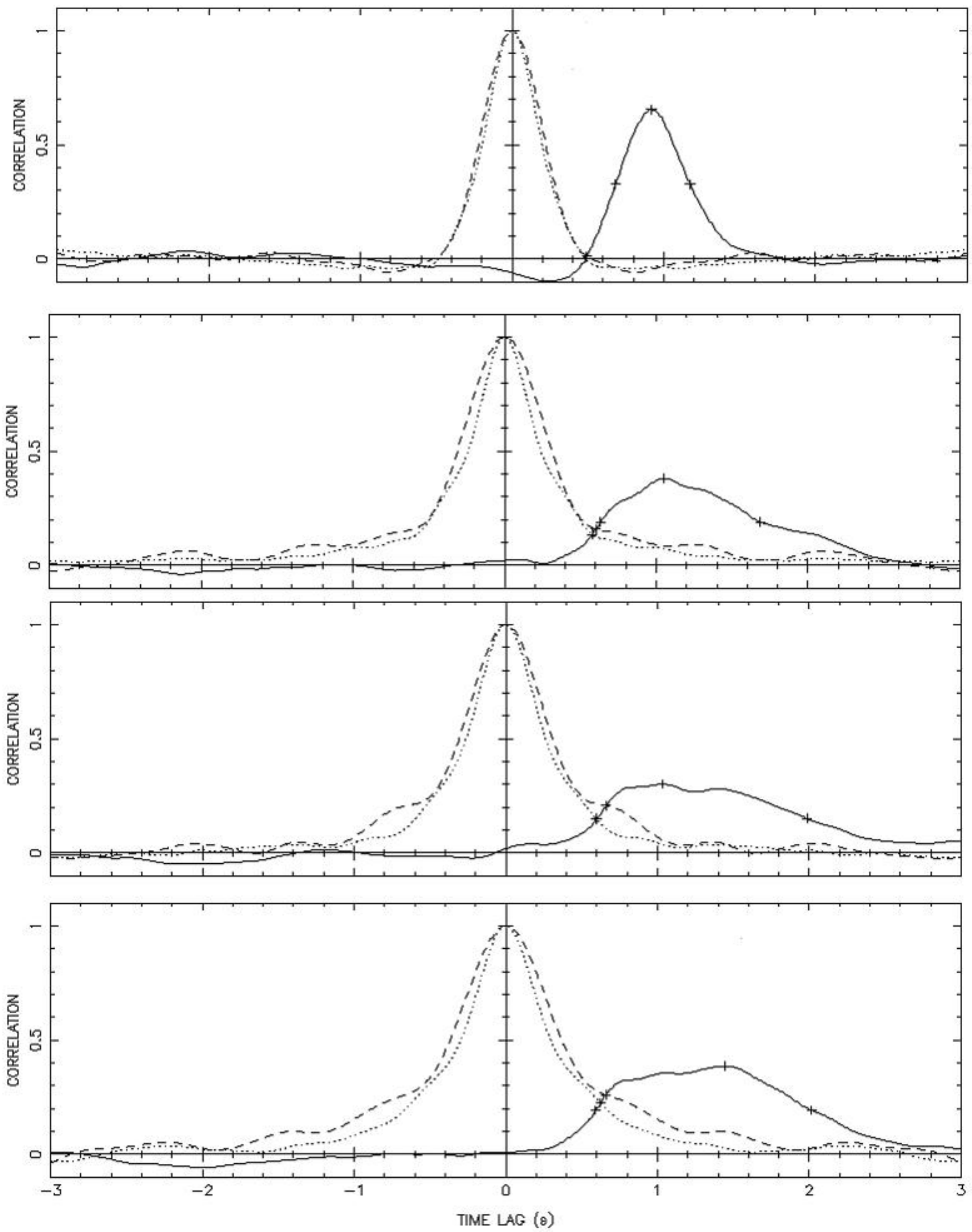

Figure 7. Cross correlation functions for the IPS observation on the 29th September 1997 for source 1150-003. Several different iCME signatures can be seen in the different cross correlations with time of observation going from 1001 UT (top image) to 1301 UT (bottom image) with there being a one hour interval between each correlation image.

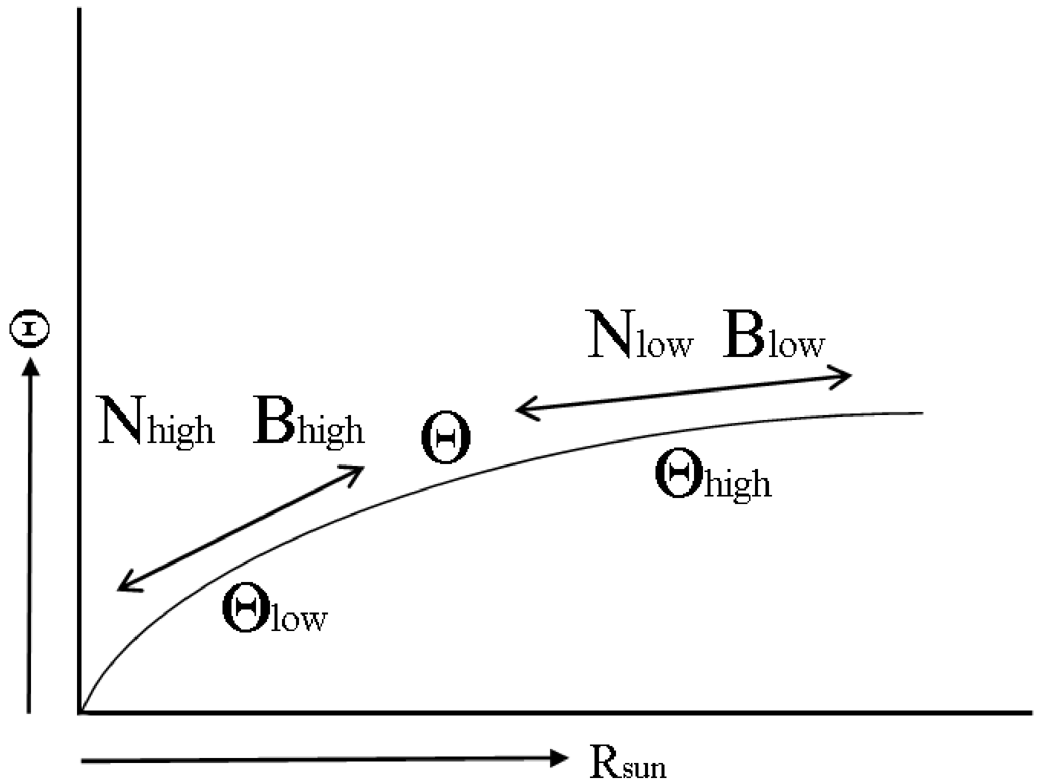

Figure 8. Solar wind density and magnetic field strength affects on iCME velocity. Θ represents spiral angle, N is solar wind density and B is solar magnetic field strength. The majority of acceleration upon iCME takes place when the spiral angle is small therefore the magnetic field strength and solar wind density is high.

Tables

LASCO CME	Feature	LASCO vel POS (kms^{-1})	Time between LASCO and IPS obs (hours)	Flight time (hours)
28/09/97	Leading edge	448	19.19	12.9
	Trailing edge	388	19.19	14.89
	Arcades	298	18.87	19.39
	Last front	486	15.77	11.89

Table 1. The different white-light features for a CME observed by LASCO on the 28th September 1997.

Date of CME	LASCO C2 vel (kms^{-1})	LASCO C3 vel (kms^{-1})	IPS vel (kms^{-1})	ΔV ($\pm$ kms^{-1})	ACE vel (kms^{-1})	Background vel (kms^{-1})
28/09/97	351	253	363	35	-	335

Table 2. ICME interaction with the background solar wind for the IPS observation on the 29th September 1997. All velocities are radial for comparison. ΔV is the spread in velocity and is used as a measure of accuracy.

[bp]

IPS observations of coronal mass ejections (CMEs)											
White-light and IPS observation times							IPS iCME characteristics				
LASCO date	LASCO vel	IPS date	Source	IPS velocity	P-point R_s	Flight time	Enhanced scint.	Temporal variations	-ve lobe	Axial ratio	Large rms_{perp}
28/09/97	298	29/09/97	1150-003	363	31	19.4	√	√	√	√	√
19/05/98	183	20/05/98	0431+206	259	37	37.2	√	√	√	√	-
15/05/00	549	16/05/00	0319+415	372	82	29.1	-	√	√	√	-
23/05/01	350	24/05/01	0431+206	508	22	12.1	√	√	√	√	√
09/05/03	656	10/05/03	0431+206	440	76	22	√	√	√	√	-
14/09/03	216	16/09/03	1229+020	560	53	47.4	√	√	√	√	√
13/05/05	1227	14/05/05	0319+415	1000	83	13	√	√	-	-	-

Table 3. IPS observations of iCMEs as they pass through the line of sight. LASCO velocities are in plane of sky whereas IPS velocities are radial. All velocities are measured in kms^{-1} and times are in hours (Hrs).

n°	Date of CME	LASCO C2 vel (kms^{-1})	LASCO C3 vel (kms^{-1})	IPS vel (kms^{-1})	ΔV ($\pm kms^{-1}$)	ACE vel (kms^{-1})	Background vel (kms^{-1})
1	28/09/97	351	253	363	35	-	335
2	20/05/98	215	310	259	6	-	400
3	15/05/00	647	785	372	66	-	340
4	23/05/01	-	350	508	16	-	343
5	09/05/03	754	-	440	13	-	390
6	14/09/03	248	757	560	52	440	357
7	13/05/05	1412	-	1000		980	581

Table 4. ICMEs interaction with the background solar wind for several IPS observations. All velocities are radial for comparison. ΔV is the spread in velocity and is used as a measure of accuracy.